

Summer Dust Aerosols Detected from CALIPSO Observations over the Tibetan Plateau

Jianping Huang¹, Patrick Minnis², Yuhong Yi³, Qiang Tang¹, Xin Wang¹,
Yongxiang Hu², Zhaoyan Liu⁴, Kirk Ayers³, Charles Trepte², and David Winker²

¹College of Atmospheric Sciences, Lanzhou University, Lanzhou, 730000

²NASA Langley Research Center, Hampton, VA, 23666

³SSAI, One Enterprise Parkway, Hampton, VA, 23666

⁴National Institute of Aerospace, Hampton, VA 23666

1 **1. Introduction**

2 Every year, deserts in eastern Asia produce a large amount of mineral dust
3 particles that become entrained in the atmosphere. These particles have been recognized
4 as important atmospheric constituents because dust particles influence the global climate
5 by scattering and absorbing solar radiation, and absorbing and emitting outgoing long-
6 wave radiation [*Tegen*, 2003; *Huang et al.*, 2006b; *Slingo et al.*, 2006]. They can also
7 cause changes in cloud properties, such as the number concentration and size of cloud
8 droplets, which can alter both cloud albedo and cloud lifetime [*Twomey et al.*, 1984;
9 *Huang et al.*, 2006a].

10 During the summer, dust from the deserts of western China, Afghanistan,
11 Pakistan, and the Middle East is transported into and stacked up against the northern and
12 southern slopes of the Tibetan Plateau. The absorption of solar radiation by dust heats up
13 the elevated surface air over the slopes. Recently, *Lau et al.* [2006a, b] pointed out that,
14 on intra-seasonal to inter-annual time scales, heating by absorbing aerosols may induce a
15 tropospheric temperature anomaly over parts of northern India and Tibet in late spring
16 and early summer, leading to an earlier onset and intensification of the Indian monsoon.
17 They proposed the importance of atmospheric heating by an “elevated heat pump” effect
18 due to dust transported from the nearby deserts to northern India stacking up against the
19 southern slopes of the Himalayas. This dust combined with the black carbon from
20 industrial and agricultural pollution in northern India provides an anomalous diabatic heat
21 source that triggers positive feedback in monsoon convective heating, enhancing the
22 Indian monsoon. These results suggest that aerosol effects on the monsoon water cycle
23 dynamics are complex and likely to be a strong function of spatial and temporal scales.

1 However, no convincing evidence of aerosol effect on monsoon climate variability has
2 been noted due to the lack of observed dust aerosol over the Tibetan area.

3 Many Asian dust studies, including ground-based lidar observations [*Murayama*
4 *et al.*, 2001; *Liu et al.*, 2002; *Sugimoto et al.*, 2003], have focused on the late winter and
5 spring due to observed long-range dust transport. There have been very few studies
6 analyzing the specific signatures of summer and fall dust storms over the Tibetan Plateau.
7 The recently launched CALIPSO satellite provides a wealth of actively sensed data over
8 the region and provides an outstanding opportunity for studying Tibetan dust storms and
9 their potential climatic effects. Unlike the current generation of space-based remote
10 sensing instruments, CALIPSO can observe aerosols over bright surfaces and beneath
11 thin clouds as well as in clear sky conditions [*Winker et al.*, 2006; *Liu et al.*, 2004;
12 *Vaughan et al.*, 2004]. This study investigates Tibetan dust characteristics and physical
13 properties using CALIPSO data. The origins of Tibetan dust storms are also examined
14 using the HYbrid Single-Particle Lagrangian Integrated Trajectory (HYSPLIT) model
15 [*Draxler*, 2006; *Escudero et al.*, 2006] (<http://www.arl.noaa.gov/ready/hysplit4.html>).

16 **2. Data**

17 The Cloud-Aerosol Lidar with Orthogonal Polarization (CALIOP) is the primary
18 instrument on the CALIPSO satellite. CALIOP is designed to acquire vertical profiles of
19 elastic backscatter at two wavelengths (532 nm and 1064 nm) from a near nadir-viewing
20 geometry during both day and night phases of the orbit. In addition to total backscatter at
21 the two wavelengths, CALIOP also provides profiles of linear depolarization at 532 nm.
22 The depolarization measurements enable the discrimination between ice and water
23 clouds, and the identification of non-spherical aerosol particles. CALIOP measurements

1 taken from June through September 2006 over Tibetan area (25 - 45°N, 75 - 100°E) are
2 obtained to calculate the volume depolarization ratio and volume color ratio profiles.
3 Note that the depolarization ratio and the color ratio are for total scattering, which is the
4 combination of particulate and molecular scattering.

5 Aura OMI (Ozone Monitoring Instrument) AAI (Absorbing Aerosol Index) data are
6 also used in this paper. The AAI indicates the presence of ultraviolet (UV)-absorbing
7 aerosols in the Earth's atmosphere, and is derived from a residual of the measured UV
8 reflectance [*Herman et al.*, 1997; *Torres et al.*, 1998; *de Graaf et al.*, 2005]. The AAI has
9 been used for a long time to remotely sense UV-absorbing aerosols, such as desert dust (e.g.,
10 *Moulin and Chiapello* [2004]).

11 **3. Results**

12 A typical example of the vertical distribution of a summer dust plume over the
13 Tibetan plateau is shown in Figure 1. On 26 July, a moderate wind and dust storm in
14 North Xinjiang and the Tarim Basin, accompanied by localized severe dust storms,
15 developed and extended southward. Under the influence of this storm, a wind-blown
16 sand and/or dust cloud persisted over northern Qinghai and Tibet through 1 August. The
17 CALIOP orbit-altitude cross section of the 532-nm total attenuated backscatter for 27
18 July 2006 at 2000 UTC in Figure 1a shows that a dust layer developed over the northern
19 slope of the Tibetan Plateau and extended from ground level to a height of 5 – 9 km
20 above mean sea level (MSL). The mineral dust layer had high values of backscatter
21 indicating that the layer was thick. Its depolarization ratio was high because it was
22 primarily composed of largely non-spherical particles. Figures 1b and 1c show the
23 vertical profiles of backscatter intensity and depolarization ratio at 39.23°N, 88.93°E (left
24 vertical line in Figure 1a) and at 37.89°N, 88.52°E (right vertical line in Figure 1a),

1 respectively. The vertical profiles of the depolarization ratio clearly show the vertical
2 structures of the dust layers over the Taklamakan desert (Figure 1b) and the northern
3 slope of the Tibetan Plateau (Figure 1c). The depolarization ratio of 20-30% indicates the
4 non-sphericity of the particles, which are assumed to be irregularly shaped dust.

5 The vertical distribution of dust plumes is one of the critical parameters in the
6 assessment of dust radiative forcing [*Claquin et al.*, 1998]. An analysis of observations
7 by *Minnis et al.* [1978] and a model study by *Carlson and Benjamin* [1980] showed that
8 an elevated Saharan dust layer could change the atmospheric heating rate dramatically.
9 *Liao and Seinfeld* [1998] claimed that clear sky long-wave radiative forcing and cloudy
10 sky top-of-atmosphere (TOA) short-wave radiative forcing are very sensitive to the
11 altitude of the dust layer. *Meloni et al.* [2005] found that SW aerosol radiative forcing at
12 the TOA has a strong dependence on aerosol vertical profiles. One of the advantages of
13 the CALIOP is that it provides a direct measure of the vertical structure of dust plumes.
14 Figure 1 shows that the dust layer extends from 4 to 6.5 km over both the Taklamakan
15 desert (Figure 1b) and the Tibetan Plateau (Figure 1c).

16 Figure 2 shows the spatial distribution of the AAI on 28 July as derived from
17 AURA satellite measurements that were taken about 12 hours later than the CALIPSO
18 data in Figure 1. It is a semi-quantitative index of the columnar absorption by aerosols at
19 0.340 μm . The signal is derived from the absorption of the upwelling Rayleigh scattering
20 from the lower strata of the atmosphere [*Herman et al.*, 1997]. It can be seen in Figure 2
21 that the large AAI center is in the area surrounding the Taklamakan desert in Xinjiang. The
22 Taklamakan desert area has a high frequency of dust storm occurrence, averaging more than
23 80 days each year. Dust aerosols from the Taklamakan Desert are entrained to an elevation of
24 5 km or higher and then transported over Tibet by the prevailing winds, which explains the

1 structure seen in Figures 1 and 2. The AAI exceeds 0.5 over most of the Tibet area and with
2 values greater than 1.0 over northern Tibet. These large values indicate that the aerosols are
3 highly absorptive.

4 To perform a statistical study of Tibetan dust plume optical properties, 10 night-
5 time cases were selected (see Table 1). Figure 3 summarizes the composite frequency
6 distributions of the volume depolarization ratio (Fig. 3a, the ratio between the parallel
7 component and the perpendicular component of the lidar backscatter) and the total
8 volume color ratio (Fig. 3b, the ratio between 1064nm lidar backscatter and 532nm lidar
9 backscatter) as functions of altitude for these cases. As shown in Figure 3a, the
10 depolarization ratio decreases significantly with increasing altitude. For lower layers at
11 altitudes from 3 to 5 km, the depolarization ratio for 64% of the pixels exceeds 20%, is
12 between 10 and 20% for 26% of the dust pixels, and is less than 10% for the remaining
13 10% of the dusty pixels. The larger depolarization ratio indicates the presence of highly
14 concentrated desert dust that is probably very irregular in shape. Note that the volume
15 depolarization ratio is particle concentration dependent, that is, the higher the dust
16 concentration, the greater the volume depolarization ratio (the closer to the particulate
17 depolarization ratio). However, the presence of spherical aerosols can reduce the dust
18 volume depolarization ratio. In the free troposphere, between 7 and 10 km, the
19 depolarization ratios for 47% of the dust pixels is less than 10% and between 10 and 20%
20 for 28% of the pixels, where the dust concentration is low relative to the molecular
21 density. The features of depolarization ratios observed in the middle troposphere,
22 between 5 and 7 km, fall between the values observed for the free and lower troposphere.
23 The depolarization ratio frequency percentages were 20%, 33% and 47% for the 0-10%,
24 10-20% and >20% ranges, respectively. In comparison to the volume depolarization

ratio, the distributions of volume color ratio with values ranging from 0.6 to 0.9 (Figure 3b) remain relatively unchanged vertically although data with low depolarization ratio values have been removed.

To investigate the dust aerosol origins, air mass trajectories were computed with the HYSPLIT model for the 10 cases listed in Table 1. Back trajectories with starting points, based on the CALIPSO observation, were computed for a 4-day period. The starting points from the back trajectory analyses (i.e., the end point of dust transport) are marked with stars in Figure 4. The horizontal trajectory curves show that the dust plumes observed over the Tibetan Plateau all originated from the Taklamakan Desert. However, the back trajectories show that the dust particles are not directly lofted to the Tibetan Plateau but that most transports occur around the anticyclonic pathway. The dust first moves eastward and then turns to the south around the edge of desert. After that the dust moves westward and accumulates over the northern slopes of the Tibetan Plateau where eventually it is lofted up over the plateau. This pathway may be related to the low thermal cyclone that occurs when dust storms are observed in the Taklamakan Desert.

4. Conclusions and Discussion

This paper presents direct Tibetan dust aerosol measurements from CALIPSO observations during summer, a season that is typically inactive for the development of dust storms. The dust particles primarily originate from the nearby Taklamakan desert and accumulate over the northern slope of the Tibetan Plateau. Because surface stations are mainly located on the eastern Tibetan Plateau, no surface observations are available over the northwestern region due to high elevation and harsh climate. However, during summer most Tibetan dust plumes develop elsewhere and are transported over western Tibet and remain

undetected from the surface. Thus, satellite remote sensing data are crucial for detecting the Tibetan dust plumes and for estimating the optical properties and radiative impacts of the particles. For example, CALIPSO detected approximately 48 Tibetan dust plumes from a total of 90 nighttime overpasses over Tibet for the period from 14 June to 30 September 2006. According to the CALIPSO observations, the frequency of occurrence of summer dust plumes over the region (25-45 °N, 75-100 °E) under study is about 53%, which is much higher than results obtained from surface observations. The total averaged dust events (floating-dust and blowing dust plus dust storm) observed from the surface stations (box region in Figure 4) is less than 10% for the 4-month period from June to September (personal communication). It is far less than the frequency detected by CALIPSO. Although the difference between CALIPSO and surface observations may be related to other factors, the CALIPSO measurements provide a wealth of previously unknown information. Of course, this study is only a first step in quantifying the effectiveness of CALIPSO for identifying dust plumes over the Tibetan Plateau. Further research should be focused on a combination of CALIPSO measurements with other NASA A-Train satellite measurements. The NASA A-Train satellites can provide near-simultaneous measurements of aerosol optical and radiative properties, cloud and aerosol vertical structure, cloud properties, and water vapor profiles. By combining TOA fluxes from the Clouds and Earth's Radiant Energy System (CERES) scanners and aerosol/cloud properties retrieved from the Moderate Resolution Imaging Spectroradiometer on *Aqua* with the vertical distributions of aerosols and clouds from CALIPSO, it should be possible to reliably determine dust aerosol radiative forcing over this remote area where heavy dust loadings occur much more frequently than expected.

1 **Acknowledgments**

2 This research is supported by National Basic Research Program of China
3 (2006CB400501) and NASA Science Mission through the CERES Project. The
4 CALIPSO data were obtained from the NASA Langley Research Center Atmospheric
5 Sciences Data Center. The OMI AAI image and data used in this study were acquired
6 using the GES-DISC Interactive Online Visualization and analysis Infrastructure as part
7 of the NASA's Goddard Earth Sciences Data and Information Services Center. The
8 authors also gratefully acknowledge the NOAA Air Resources Laboratory for the
9 provision of the HYSPLIT transport and dispersion model and/or READY website
10 (<http://www.arl.noaa.gov/ready.html>) used in this publication.

11

References

- Carlson, T. N., and S. G. Benjamin (1980), Radiative heating rates for Saharan dust, *J. Atmos. Sci.*, *37*(1), 193–213.
- Claquin, T., et al. (1998), Uncertainties in assessing radiative forcing by mineral dust, *Tellus B*, *50*(5), 491–505, doi:10.1034/j.1600-0889.1998.t01-2-00007.x.
- de Graaf, M., et al. (2005), Absorbing Aerosol Index: Sensitivity analysis, application to GOME and comparison with TOMS, *J. Geophys. Res.*, *110*, D01201, doi:10.1029/2004JD005178.
- Draxler, R.R. (2006), The use of global and mesoscale meteorological model data to predict the transport and dispersion of tracer plumes over Washington, D.C., *Weather and Forecasting*, *21*(3), 383–394, doi:10.1175/WAF926.1.
- Escudero, M., et al. (2006), Determination of the contribution of northern Africa dust source areas to PM₁₀ concentrations over the central Iberian Peninsula using the Hybrid Single-Particle Lagrangian Integrated Trajectory model (HYSPLIT) model, *J. Geophys. Res.*, *111*, D06210, doi:10.1029/2005JD006395.
- Herman, J. R., et al. (1997), Global distribution of UV-absorbing aerosols from Nimbus 7/TOMS data, *J. Geophys. Res.*, *102*(D14), 16,911–16,922.
- Huang, J., et al. (2006a), Possible influences of Asian dust aerosols on cloud properties and radiative forcing observed from MODIS and CERES, *Geophys. Res. Lett.*, *33*, L06824, doi:10.1029/2005GL024724.
- Huang, J., et al. (2006b), Satellite-based assessment of possible dust aerosols semi-direct effect on cloud water path over East Asia, *Geophys. Res. Lett.*, *33*, L19802, doi:10.1029/2006GL026561.

- 1 Lau, K.-M., et al. (2006a), Asian monsoon anomalies induced by aerosol direct effects,
2 *Climate Dynamics*, 26(7-8), 855-864, doi:10.1007/s00382-006-0114-z.
- 3 Lau, K.-M., and K.-M. Kim (2006b), Observational relationships between aerosol and
4 Asian monsoon rainfall, and circulation, *Geophys. Res. Lett.*, 33, L21810,
5 doi:10.1029/2006GL027546.
- 6 Liao, H., and J.H. Seinfeld (1998), Radiative forcing by mineral dust aerosols: Sensitivity
7 to key variables, *J. Geophys. Res.*, 103(D24), 31,637-31,646.
- 8 Liu, Z., et al. (2002), Extinction-to-backscatter ratio of Asian dust observed by high-
9 spectral-resolution lidar and Raman lidar, *Applied Optics*, 41(15), 2760-2767.
- 10 Liu, Z., et al. (2004), Use of probability distribution functions for discriminating between
11 cloud and aerosol in lidar backscatter data, *J. Geophys. Res.*, 109, D15202,
12 doi:10.1029/2004JD004732.
- 13 Meloni, D., et al. (2005), Influence of the vertical profile of Saharan dust on the visible
14 direct radiative forcing, *Journal of Quantitative Spectroscopy Radiative Transfer*,
15 93(4), 497-413, doi:10.1016/j.jqsrt.2004.08.035.
- 16 Minnis, P. and S. K. Cox (1978), Magnitude of the radiative effects of the Sahara dust
17 layer, *Atmospheric Science Paper No. 283*, Colorado State University, Ft. Collins,
18 Colorado, January, 111 pp.
- 19 Moulin, C., and I. Chiapello (2004), Evidence of the control of summer atmospheric
20 transport of African dust over the Atlantic by Sahel sources from TOMS satellites
21 (1979–2000), *Geophys. Res. Lett.*, 31, L02107, doi:10.1029/2003GL018931.
- 22 Murayama, T., et al. (2001), Ground-based network observation of Asian dust events of
23 April 1998 in east Asia, *J. Geophys. Res.*, 106(D16), 18,345–18,360.

1 Slingo, A., et al. (2006), Observations of the impact of a major Saharan dust storm on the
2 atmospheric radiation balance, *Geophys. Res. Lett.*, 33, L24817,
3 doi:10.1029/2006GL027869.

4 Sugimoto, N., et al. (2003), Record heavy Asian dust in Beijing in 2002: Observations
5 and model analysis of recent events, *Geophys. Res. Lett.*, 30(12), 1640,
6 doi:10.1029/2002GL016349.

7 Tegen, I. (2003), Modeling the mineral dust aerosol cycle in the climate system, *Quat.*
8 *Sci. Rev.*, 22(19), 1821 – 1834, doi:10.1016/S0277-3791(03)00163-X.

9 Torres, O., et al. (1998), Derivation of aerosol properties from satellite measurements of
10 backscattered ultraviolet radiation: Theoretical basis, *J. Geophys. Res.*, 103(D14),
11 17,099–17,110.

12 Twomey, S., et al. (1984), An assessment of the impact of pollution on global cloud
13 albedo, *Tellus B*, 36, 356-366.

14 Vaughan, M., et al. (2004), Fully automated analysis of space-based lidar data: an
15 overview of the CALIPSO retrieval algorithms and data products, *Proc. SPIE*,
16 5575, 16-30, doi:10.1117/12.572024.

17 Winker, D. M., et al. (2006), The CALIPSO mission and initial results from CALIOP,
18 *Proc. SPIE*, 6409, 640902, doi:10.1117/12.698003.

19

1
2

Table 1. Summer Tibetan dust storm cases selected from June to September 2006

Case	Date	Start Point of Backward Trajectory	Ground Height at Start Point (m)
1	June 27, 2006	36.67 °N, 91.25 °E	4611.6
	July 9, 2006	36.00 °N, 85.00 °E	4979.0
3	July 27, 2006	36.11 °N, 87.99 °E	4995.6
4	July 30, 2006	36.11 °N, 80.26 °E	4297.1
5	August 1, 2006	34.92 °N, 83.01 °E	5239.8
6	August 12, 2006	36.11 °N, 87.97 °E	5006.7
7	August 19, 2006	36.11 °N, 86.43 °E	5040.1
8	September 4, 2006	37.57 °N, 86.62 °E	3516.8
9	September 6, 2006	36.11 °N, 89.48 °E	4914.2
10	September 20, 2006	36.41 °N, 86.46 °E	4938.7

3

4

Figure Captions

Figure 1 a) The altitude-orbit cross-section of total attenuated backscattering intensity over Taklamkan-Tibet Plateau; (b) the vertical profiles of total 532 nm attenuated backscattering intensity (black curve) and depolarization ratio (green curve) about 20 GMT on 27 July 2006 at 39.23°N, 88.93°E; and (c) same as (b) but for 37.89°N, 88.52°E.

Figure 2 Aura OMI aerosol index over Taklamkan Desert and Tibet Plateau on 28 July 2006.

Figure 3 Frequency distribution of the depolarization ratio (a) and the color ratio (b) as functions of altitude for the 10 selected cases.

Figure 4 Four-day back trajectories of air parcels climbing upon the Tibet Plateau for the 10 cases listed in Table 1. The gray dots represent surface observation stations.

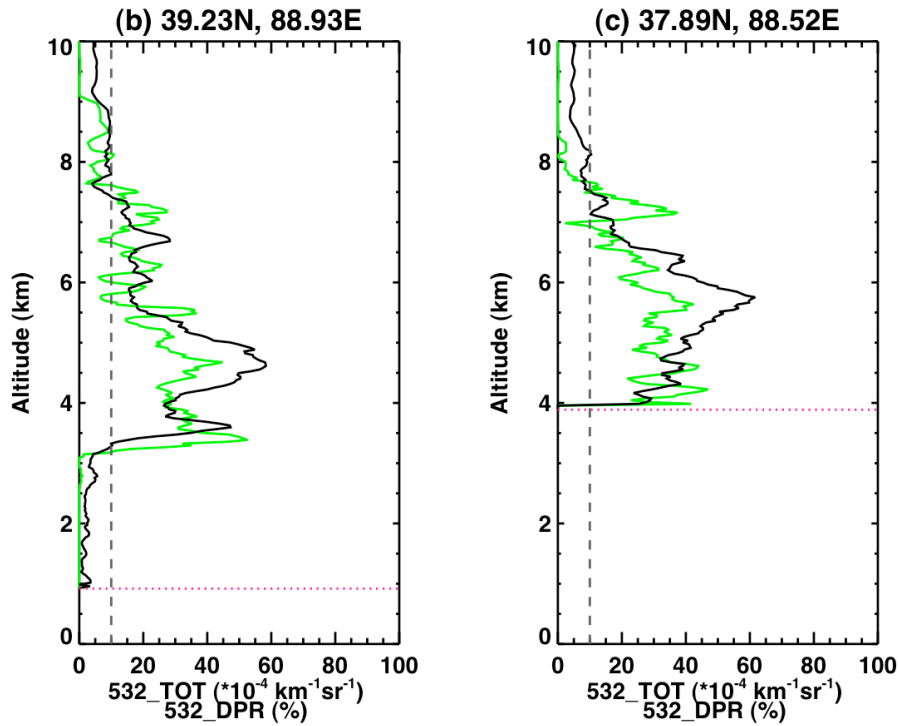
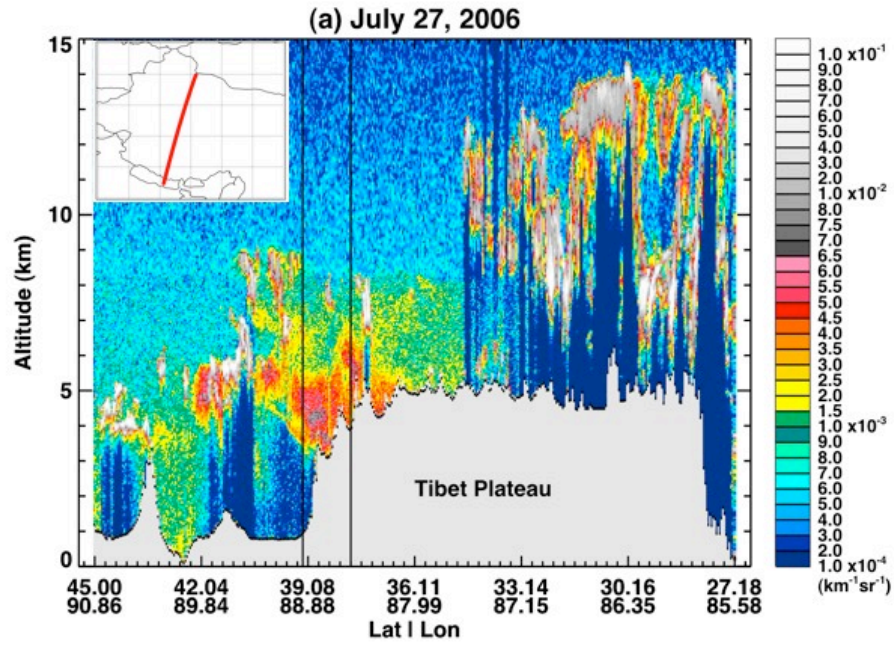


Figure 1 a) The altitude-orbit cross-section of total attenuated backscattering intensity over Taklamkan-Tibet Plateau; (b) the vertical profiles of total 532 nm attenuated backscattering intensity (black curve) and depolarization ratio (green curve) about 20 GMT on 27 July 2006 at 39.23°N, 88.93°E; and (c) same as (b) but for 37.89°N, 88.52°E.

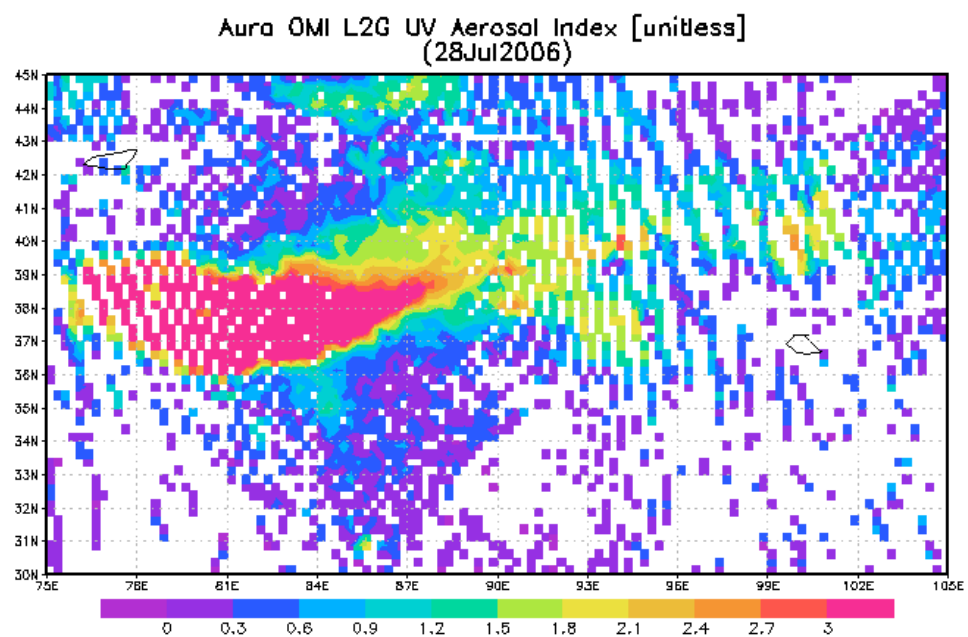
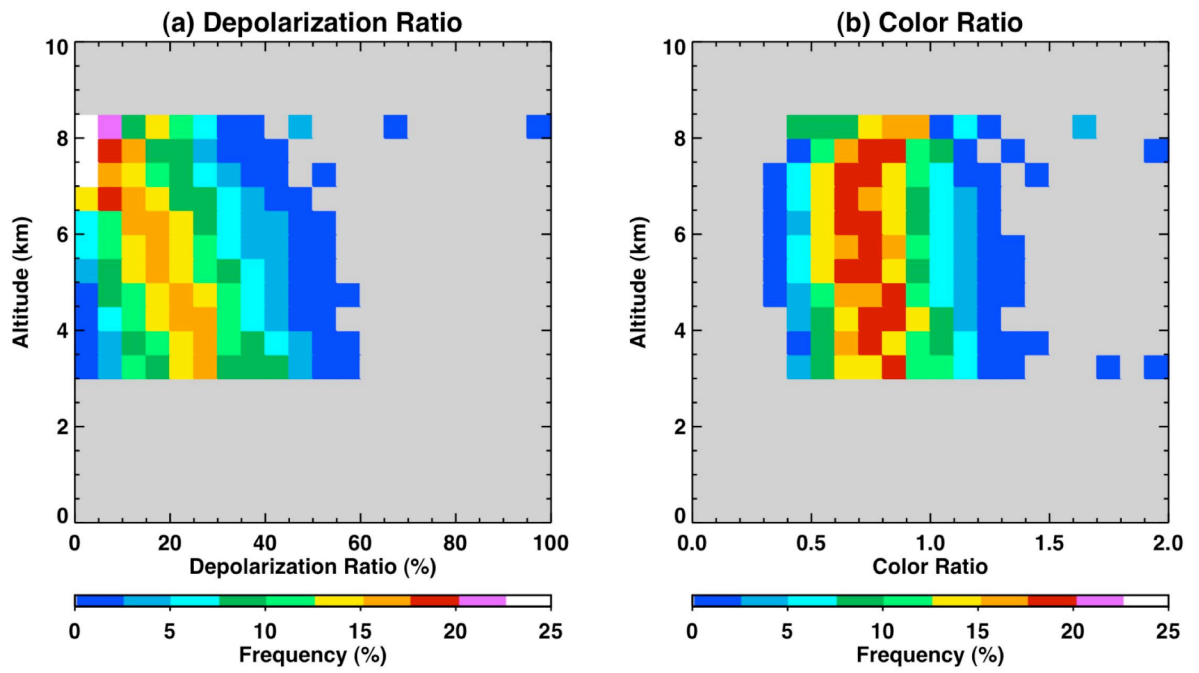
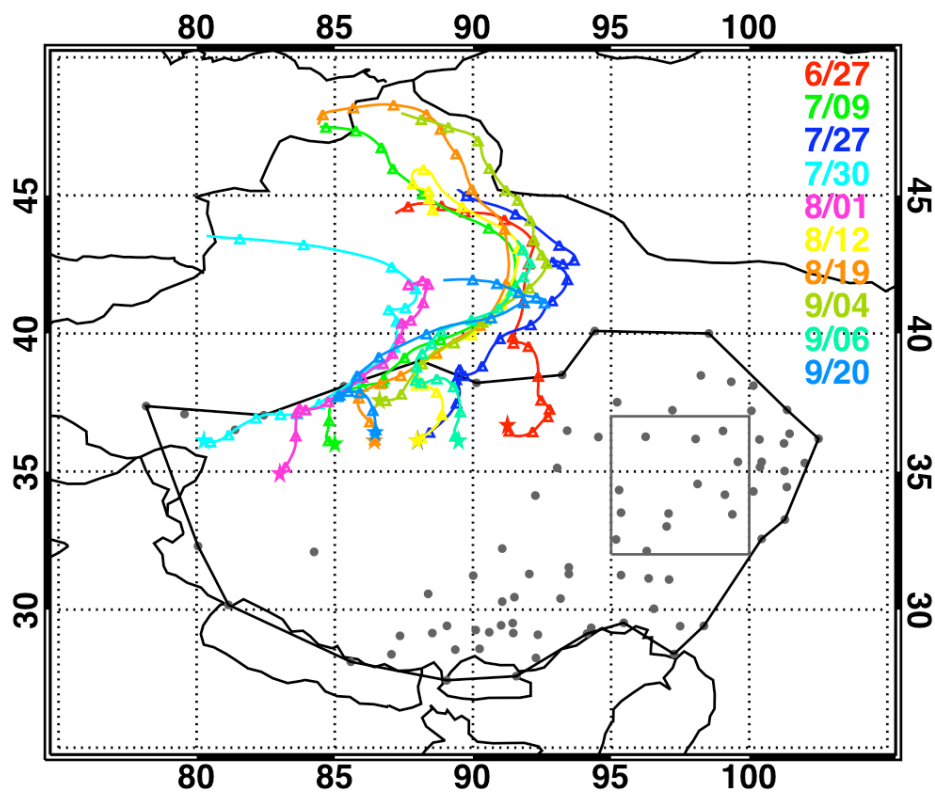


Figure 2. Aura OMI aerosol index over Taklamkan Desert and Tibet Plateau on 28 July 2006.



1
2 Figure 3 Frequency distribution of the depolarization ratio (a) and the color ratio (b) as
3 functions of altitude for the 10 selected cases.
4
5

1
2



3
4
5
6
7

Figure 4 Four-day back trajectories of air parcels climbing upon the Tibet Plateau for the 10 cases listed in Table 1. The gray dots represent surface observation stations.

8
9

10